Supplement to Revisiting the contribution of land transport and shipping emissions to tropospheric ozone

Mariano Mertens
Institut für Physik der Atmosphäre
DLR-Oberpfaffenhofen

mariano.mertens@dlr.de

February 2018

Contents

S1 Discussion about uncertainties in radiative forcing calculations

The radiative forcing (RF) of (tropospheric) ozone since pre-industrial time is estimated by calculating the radiative flux change between the results of a simulation with preindustrial and one with present day conditions (c.f. Fig. S1). To calculate not the total RF, but the RF caused only by a specific emission source (e.g. land transport) usually the radiative flux change between the results of one simulation with and one simulation without emissions is calculated (perturbation approach). In some cases not a 100 % perturbation but e.g. a 5 % perturbation is chosen, which is then usually scaled to 100 %. However, using the perturbation approach the RFs calculated by perturbing different emission sources are not necessarily additive (e.g. Grewe et al., 2012). Accordingly, the RFs calculated for different anthropogenic sources does not add up to the total tropospheric ozone RF (see Fig. S1)

The approach of calculating the RF by using the results of the tagging method is slightly different. Here, the ozone field is completely decomposed into contributions of x emission sources (see also Dahlmann et al., 2011). For each of these x emission sources a radiative flux change between O_3 and O_3-O_3^x is calculated (see manuscript for details).

Compared to the 'classical' approach by comparing preindustrial times and present day this approach has two assumptions:

1. The sum of all non-anthropogenic categories corresponds to the pre-industrial ozone,
2. The sum of the RFs from all n individual categories corresponds total RF ($\sum_i^n RF_i = RF$).

Two reasons exist why the first assumption is not completely fulfilled. First, due to additional anthropogenic emissions the ozone production efficiency of the non-anthropogenic emissions is decreased and the same amounts of non-anthropogenic emissions produce less ozone. Second, a present day climate is assumed and therefore the influence of the climate onto ozone (and the associated RF) is not considered.

Gauss et al. (2006) gives an difference of the ozone column between present day and past climate, using preindustrial emissions, below 1 DU for the tropospheric ozone column (case 1 - 1c discussed by Gauss et al., 2006). The impact of the climate on the radiative forcing is around 10 % (comparing the results of (case 2- case 1c) and (case 2 - case 1)). With respect to the first reason, Gauss et al. (2006) reports an anthropogenic change of the tropospheric ozone column of roughly 10 DU. Our simulation results (see Fig. S2) shows a contribution of the categories anthropogenic non-traffic, land transport, shipping, and aviation of roughly 10 DU. However, also the categories of methane degradation, biomass burning and biogenic are partly influenced by anthropogenic activities. These contributions are delicate to quantify. Accordingly, the total anthropogenic contribution to the tropospheric ozone column as estimated by the tagging approach is slightly larger as the 10 DU. We estimate the maximum difference between the non-anthropogenic caused ozone in our simulation results and the preindustrial ozone of roughly 20 %.

Concerning the second assumption, Dahlmann et al. (2011) showed that $\sum_i^n RF_i$ is around 10 % lower as the RF using the whole O_3 field.

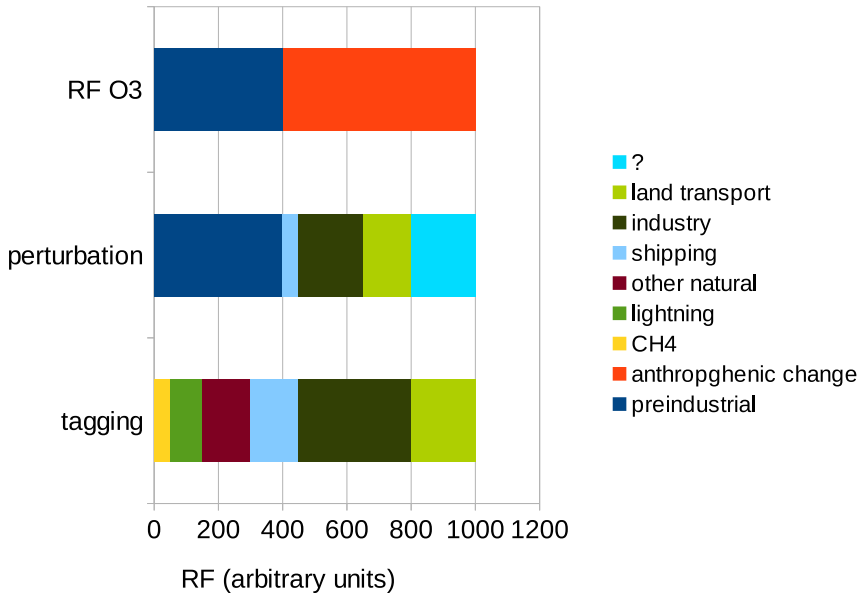

Figure S1: Simplified sketch of three different ways to calculate RFs. 'RF O3' shows the classical way of calculating the anthropogenic RF by calculating the radiative flux of a preindustrial simulation and a simulation with all emissions. 'Perturbation' shows the perturbation approach, here the RF of different emission sources is estimated by perturbation simulations turning specific emissions off. This approach, however, leads to a part of ozone which cannot be attributed to one sector (marked with ?). This is mainly caused by changes of the ozone production efficiency. The 'tagging' method estimates a radiative forcing for every specific category. Accordingly, a complete attribution of the RF to specific emission sources is possible.

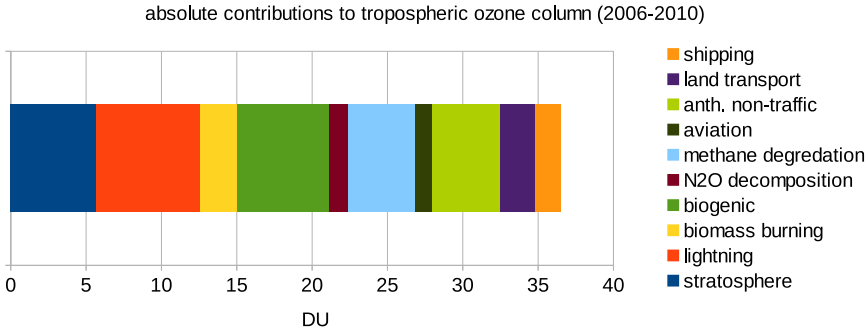

Figure S2: Multi-annual global average (2006–2010) of the contribution to the tropospheric ozone column (using the WMO tropopause definition) for the results of the *base* simulation.

S2 Comparison of Γ for Tagging and Perturbation approach

To compare the perturbation and the tagging results Γ is calculated for O_3 and for O_3^{tra}:

$$\Gamma^{O3} = \frac{P_{O3}^{lin}(NO_x = 0)}{P_{O3}^{lin}(NO_x = \text{unperturbed})} \quad (1)$$

$$\Gamma^{O3tra} = \frac{P_{O3}tra^{lin}(NO_y^{tra} = 0)}{P_{O3}tra^{lin}(NO_y^{tra} = \text{unperturbed})} \quad (2)$$

Γ^{O3} is defined in terms of the changes of the net ozone production (P_{O3}) if NO_x emissions are changed, investigating the response of the impact as analysed by the perturbation method. Γ^{O3tra} is defined in terms of the linearised change the net O_3 production for the tagged category land transport ($P_{O3}tra^{lin}$) if NO_y^{tra} is changed. Figure S3 shows how the linearised ozone production rates are calculated (more details are given in the manuscript). Figure S3b shows the are averaged production rates and NO_x mixing ratios. The tangent is approximated using the results of the perturbed and the unperturbed simulation (Fig. S3c). The same was performed for NO_y^{tra} and $P_{O3}tra$ (see Fig. S3d).

Of the four considered regions (see Table S1) North Africa and South America shows a response of the O_3 chemistry which is closest to linear ($\Gamma^{O3} = 0.2 - 0.3$). In these regions Γ^{O3tra} is almost identical and the difference between perturbation and tagging is rather low. In South-east Asia and Europe, however, the chemistry is mainly in the non-linear or saturated regime. Accordingly, Γ^{O3} is larger compared to Γ^{O3tra}, meaning that the contribution response much more linear compared to the impact.

Table S1: Comparison of Γ (definition see text) between O_3 and O_3^{tra} for different regions.

	ΓO_3	ΓO_3^{tra}
Europe	0.9	0.6
South-east Asia	0.6	0.3
North Africa	0.4	0.3
South America	0.3	0.2

Table S2: Definition of the geographical areas used for the analyses performed in Sect. 4.

	latitude	longitude
Europe	45 – 55	0 – 20
South-east Asia	20 – 30	100 – 120
North Africa	0 – 40	240 – 290
South America	0 – 30	-10 – 30

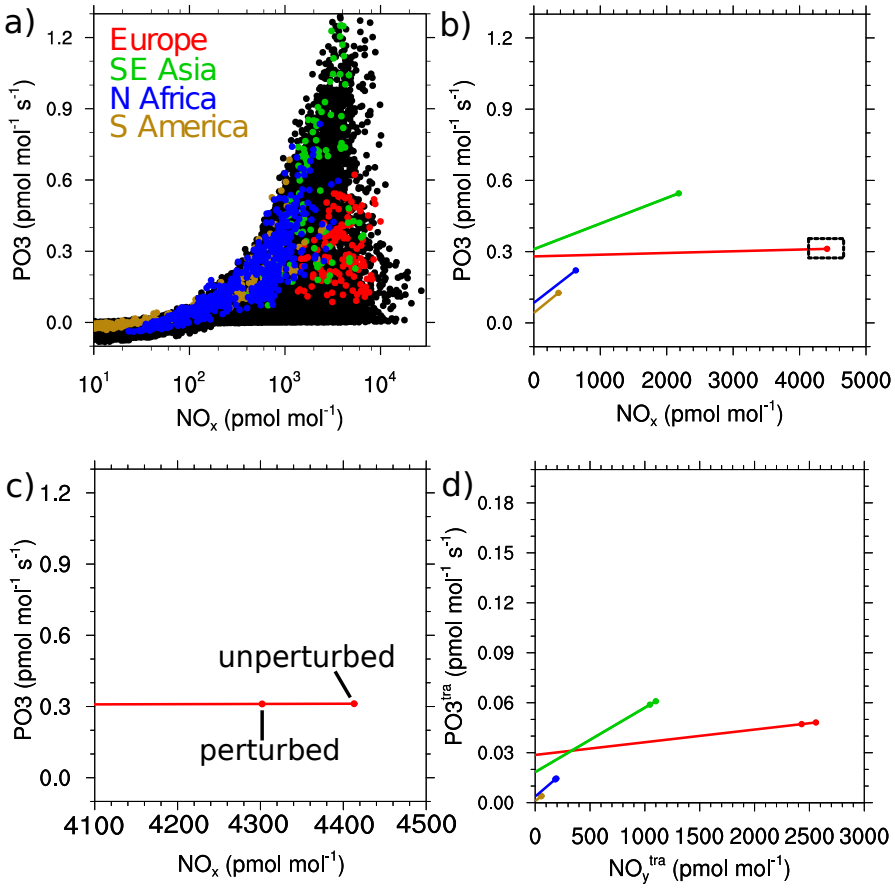

Figure S3: Dependency between NO_x mixing ratios and net O_3 production. (a) Gridbox values: The black dots represent monthly mean values at ground level for the year 2010 of every individual grid box. The individual colours indicate monthly average values during May–August (Northern Hemisphere) and November–February (Southern Hemisphere) for individual regions (defined as rectangular areas, see Table S2). (b) Regional values: The single dots represent year 2010 averages for the four regions shown in (a). In addition the tangents were calculated for every region by comparing the perturbed and the unperturbed simulations. The black rectangle highlights the region shown in (c). (d) is as (b) but showing the tagged tracers NO_y^{tra} (NO_y from land transport emissions) and the associated net O_3 production rate. The x-axes of (b), (c) and, (d) are linear, while (a) uses a logarithmic x-axis.

S3 O_3 shares estimated by the tagging method and the perturbation approach

Fig. S4 shows zonal average values of the individual O_3 shares comparing the tagging and the perturbation approach. In general, the O_3 shares estimates by the tagging approach are much larger as estimated by the perturbation approach.

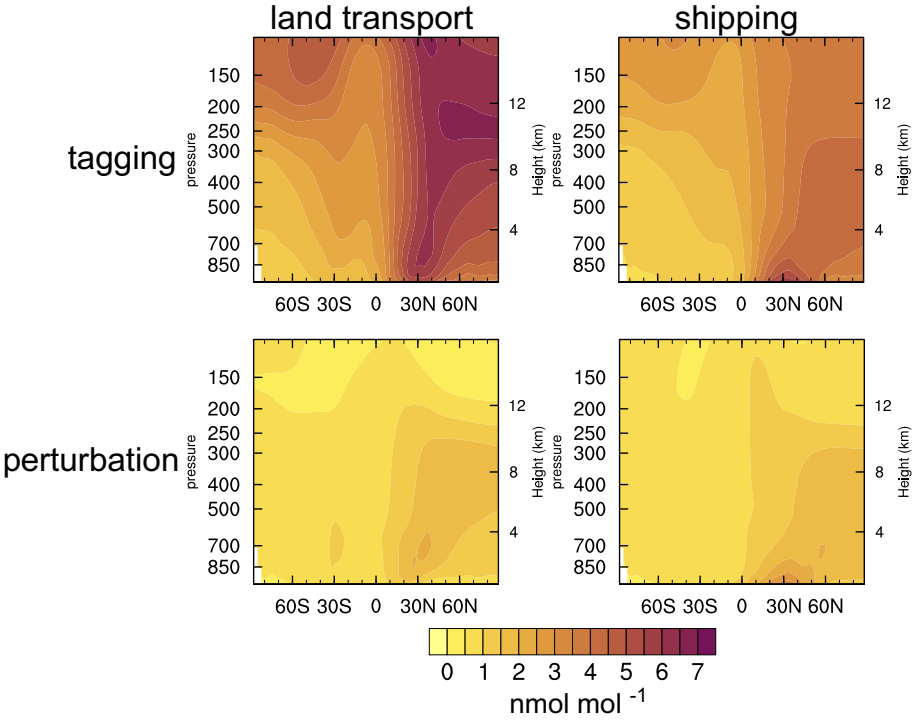

Figure S4: Multi-annual zonal average (2006–2010) of O_3 shares as estimated by the perturbation method and the tagging approach. Shown are the contribution and impact of the land transport and shipping emissions to ozone, as estimated by the tagging method and the perturbation approach, respectively.

S4 July mean values

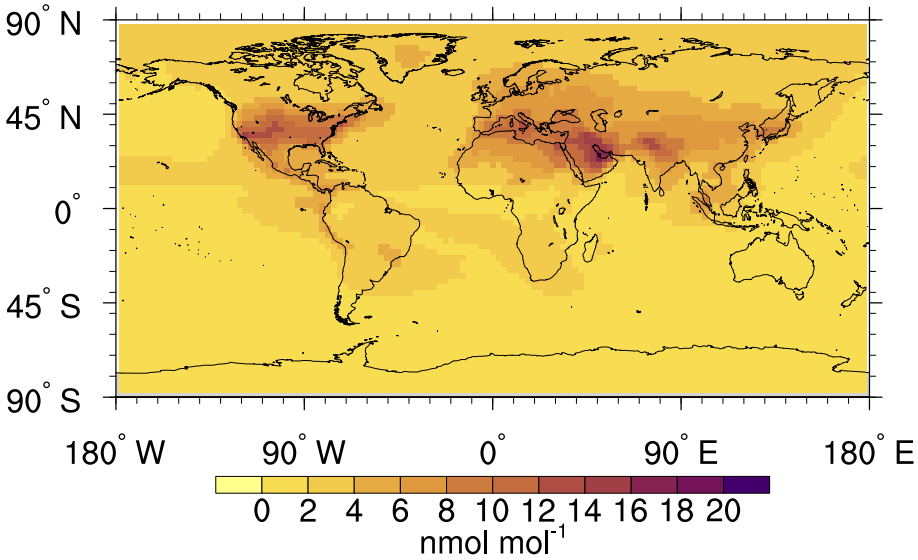

Figure S5: Multi-annual average (2006–2010) of the absolute contribution of road traffic emissions (O_3^{tra}, in nmol mol^{-1}) for July.

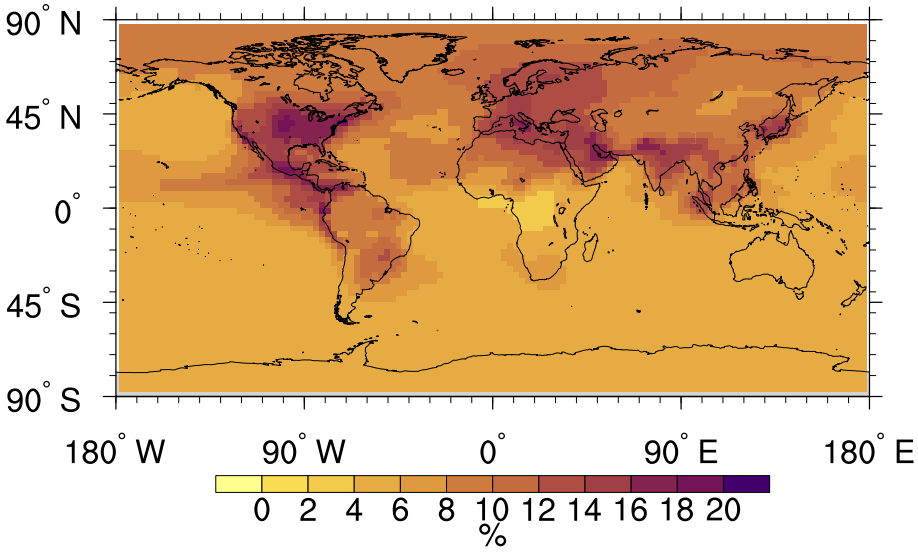

Figure S6: Multi-annual average (2006–2010) of the absolute contributions of road traffic emissions (O_3^{tra} in %) for July.

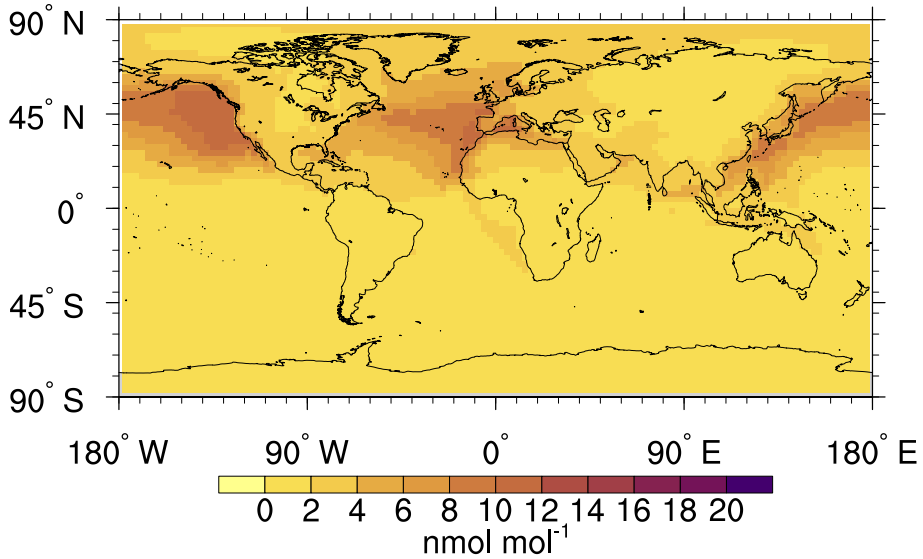

Figure S7: Multi-annual average (2006–2010) of the absolute contribution of shipping emissions (O_3^{shp}, in nmol mol^{-1}) for July.

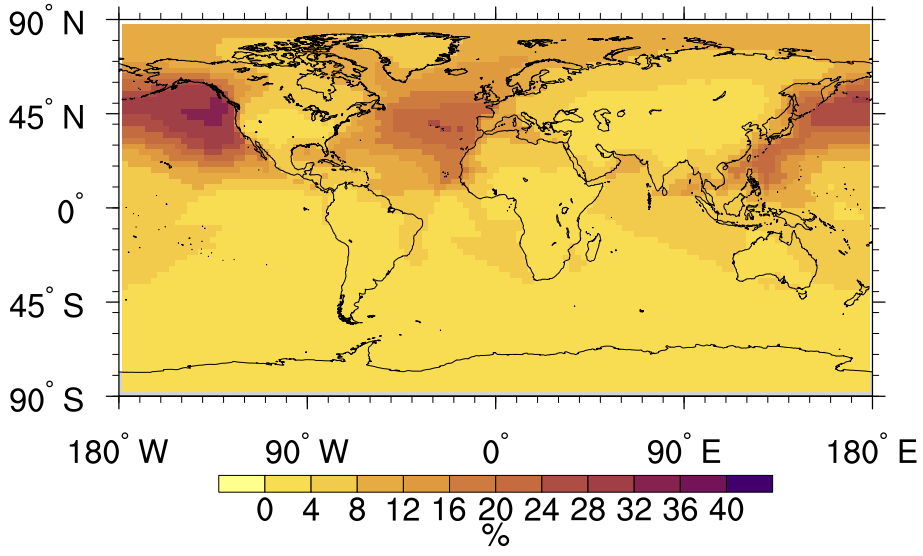

Figure S8: Multi-annual average (2006–2010) of the relative contribution of shipping emissions (O_3^{shp}, in %) for July.

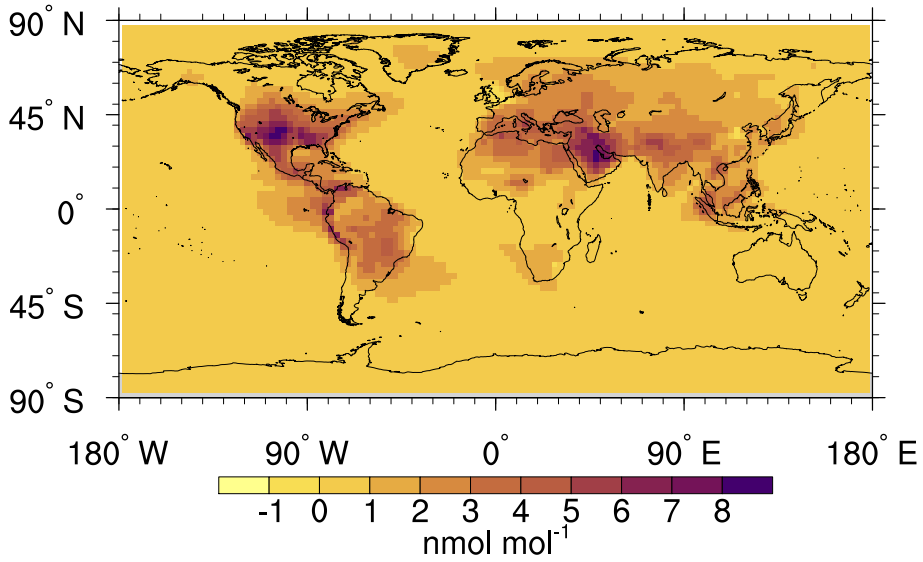

Figure S9: Multi-annual average (2006–2010) of the absolute impact of road traffic emissions (in nmol mol^{-1}) for July. Values are diagnosed using a 5 % perturbation.

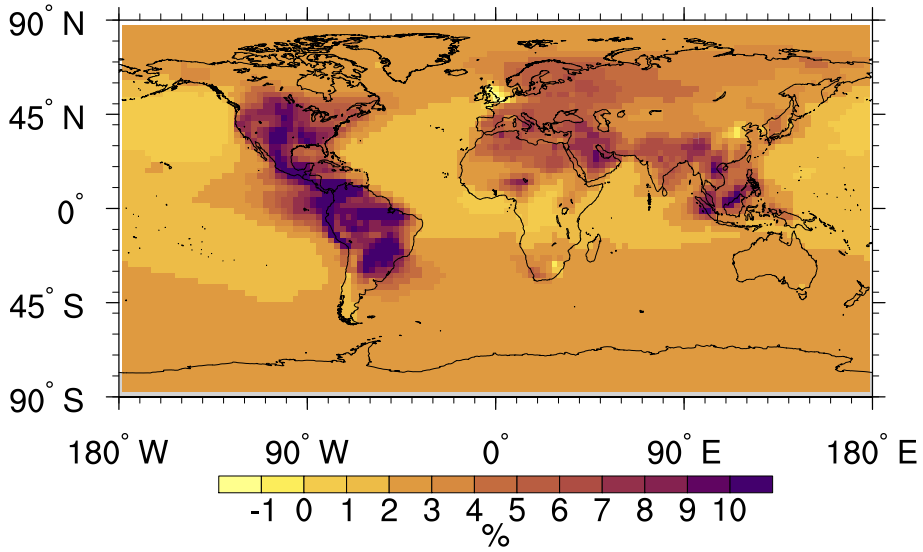

Figure S10: Multi-annual average (2006–2010) of the relative impact of road traffic emissions (in %) for July. Values are diagnosed using a 5 % perturbation.

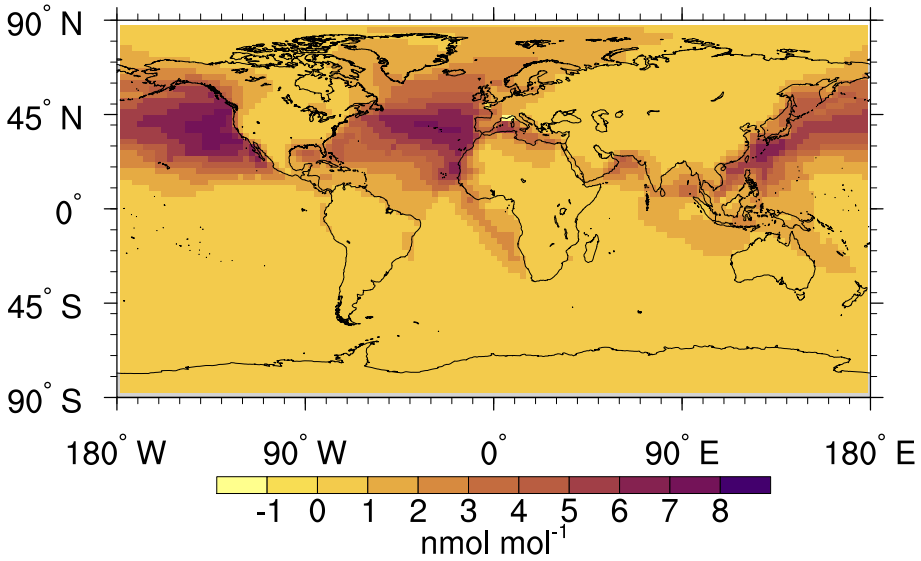

Figure S11: Multi-annual average (2006–2010) of the absolute impact of shipping emissions (in nmol mol^{-1}) for July. Values are diagnosed using a 5 % perturbation.

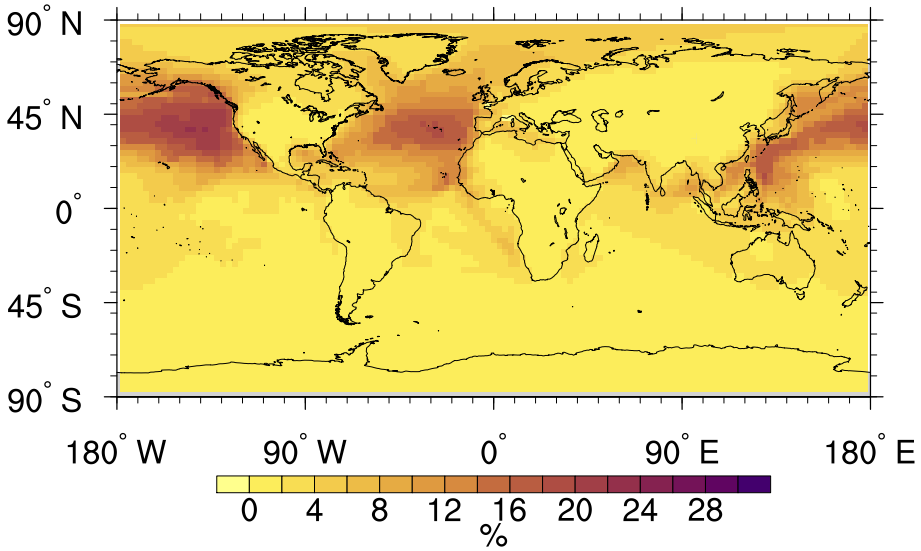

Figure S12: Multi-annual average (2006–2010) of the relative impact of shipping emissions (in %) for July. Values are diagnosed using a 5 % perturbation.

S5 Comparision to RC1SD-base10a simulation

The following figures show the difference between the *BASE* simulation and the RC1SD-base10a simulation described by Jöckel et al. (2016).

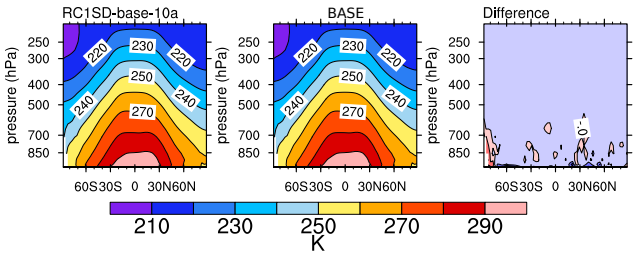

Figure S13: Zonal averaged temperature (in K) for 2005–2010. The left plot shows the value for the RC1SD-base10a, the middle plot the value for the simulation *BASE* and the right plot the absolute difference between the two fields. The colour bar indicates only the values for the first two plots.

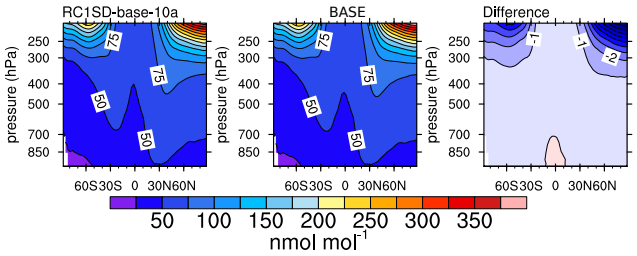

Figure S14: As figure S13 but for O_3 (in nmol mol^{-1}).

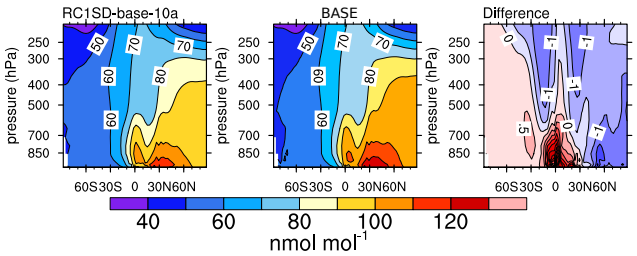

Figure S15: As figure S13 but for CO (in nmol mol^{-1}).

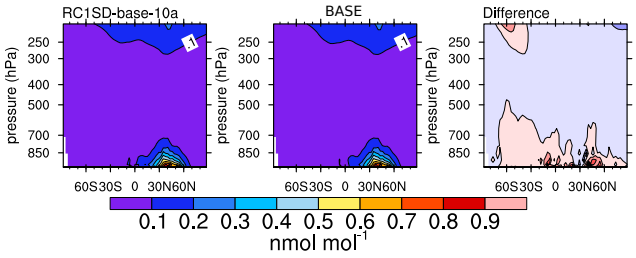

Figure S16: As figure S13 but for NO_x (in nmol mol^{-1}).

S6 References

References

Dahlmann, K., Grewe, V., Ponater, M., and Matthes, S.: Quantifying the contributions of individual NOx sources to the trend in ozone radiative forcing, Atmos. Environ., 45, 2860–2868, doi:http://dx.doi.org/10.1016/j.atmosenv.2011.02.071, URL http://www.sciencedirect.com/science/article/pii/S1352231011002366, 2011.

Gauss, M., Isaksen, I. S. A., Lee, D. S., and Søvde, O. A.: Impact of aircraft NOx emissions on the atmosphere – tradeoffs to reduce the impact, Atmospheric Chemistry and Physics, 6, 1529–1548, doi:10.5194/acp-6-1529-2006, URL http://www.atmos-chem-phys.net/6/1529/2006/, 2006.

Grewe, V., Dahlmann, K., Matthes, S., and Steinbrecht, W.: Attributing ozone to NOx emissions: Implications for climate mitigation measures, Atmos. Environ., 59, 102–107, doi:10.1016/j.atmosenv.2012.05.002, URL http://www.sciencedirect.com/science/article/pii/S1352231012004335, 2012.

Jöckel, P., Tost, H., Pozzer, A., Kunze, M., Kirner, O., Brenninkmeijer, C. A. M., Brinkop, S., Cai, D. S., Dyroff, C., Eckstein, J., Frank, F., Garny, H., Gottschaldt, K.-D., Graf, P., Grewe, V., Kerkweg, A., Kern, B., Matthes, S., Mertens, M., Meul, S., Neumaier, M., Nützel, M., Oberländer-Hayn, S., Ruhnke, R., Runde, T., Sander, R., Scharffe, D., and Zahn, A.: Earth System Chemistry integrated Modelling (ESCiMo) with the Modular Earth Submodel System (MESSy) version 2.51, Geosci. Model Dev., 9, 1153–1200, doi:10.5194/gmd-9-1153-2016, URL http://www.geosci-model-dev.net/9/1153/2016/, 2016.